Molecular Neurobiology (2021) 58:2508–2522
https://doi.org/10.1007/s12035-021-02285-1

Modulators of Neuroinflammation Have a Beneficial Effect in a Lafora Disease Mouse Model

Belén Mollá [1,2] · Miguel Heredia [1,2] · Pascual Sanz [1,2]

Received: 9 November 2020 / Accepted: 7 January 2021 / Published online: 14 January 2021
© The Author(s), under exclusive licence to Springer Science+Business Media, LLC part of Springer Nature 2021

Abstract

Lafora disease (LD; OMIM#274780) is a fatal rare neurodegenerative disorder characterized by generalized epileptic seizures and the presence of polyglucosan inclusions (PGs), called Lafora bodies (LBs), typically in the brain. LD is caused by mutations in two genes *EPM2A* or *EPM2B*, which encode respectively laforin, a glucan phosphatase, and malin, an E3-ubiquitin ligase. Much remains unknown about the molecular bases of LD and, unfortunately, appropriate treatment is still missing; therefore patients die within 10 years from the onset of the disease. Recently, we have identified neuroinflammation as one of the initial determinants in LD. In this work, we have investigated anti-inflammatory treatments as potential therapies in LD. With this aim, we have performed a preclinical study in an *Epm2b−/−* mouse model with propranolol, a β-adrenergic antagonist, and epigallocatechin gallate (EGCG), an antioxidant from green tea extract, both of which displaying additional anti-inflammatory properties. In vivo motor and cognitive behavioral tests and ex vivo histopathological brain analyses were used as parameters to assess the therapeutic potential of propranolol and EGCG. After 2 months of treatment, we observed an improvement not only in attention defects but also in neuronal disorganization, astrogliosis, and microgliosis present in the hippocampus of *Epm2b−/−* mice. In general, propranolol intervention was more effective than EGCG in preventing the appearance of astrocyte and microglia reactivity. In summary, our results confirm the potential therapeutic effectiveness of the modulators of inflammation as novel treatments in Lafora disease.

Keywords Lafora disease · Neuroinflammation · Reactive astrocytes, activated microglia, propranolol · Epigallocatechin gallate (EGCG)

Introduction

Progressive myoclonus epilepsy of the Lafora type (Lafora disease, LD; OMIM#254780) is a fatal rare neurodegenerative disease of the childhood characterized by generalized epileptic seizures, cognitive decline, and rapid deterioration towards a vegetative state. Unfortunately, an effective treatment is still missing and patients irredeemably die within 10 years from onset [1]. The hallmark of LD is the presence of insoluble polyglucosan inclusions, called Lafora bodies (LBs), in the brain and other peripheral tissues [2, 3], which are associated with the symptomatology and fatal progression.

LD is an autosomal recessive disorder mainly caused by mutations in either *EPM2A* or *EPM2B/NHLRC1* genes [4–6]. These genes respectively encode laforin, a glucan phosphatase, and malin, an E3-ubiquitin ligase. Despite the disparity in their enzymatic function, there is evidence that laforin and malin assemble into a functional complex involved in glycogen metabolism [7–9], as part of a quality control mechanism to prevent the accumulation of insoluble glycogen [10, 11]. Due to this collaborative function, the symptomatology is indistinguishable in patients harboring either laforin or malin mutations.

Throughout LD history (from 1911 to 2020), only around 250 patients have been diagnosed worldwide thus human samples are scarce and pathophysiological studies are

✉ Belén Mollá
bmolla@ibv.csic.es

Miguel Heredia
mheredia@ibv.csic.es

Pascual Sanz
sanz@ibv.csic.es

[1] Laboratory of Nutrient Signaling, Institute of Biomedicine of Valencia (CSIC), Consejo Superior de Investigaciones Científicas, Jaime Roig 11, 46010 Valencia, Spain

[2] Centro de Investigación Biomédica en Red de Enfermedades Raras (CIBERER), 46010 Valencia, Spain

insufficient. As a result, in vitro and in vivo models of LD have become of paramount importance when it comes to gain knowledge on the pathogenesis. Different knockout (KO) mouse models have been generated to achieve a complete loss of function of laforin (*Epm2a*−/−) [12] or malin (*Epm2b*−/−) [13–15]. Both *Epm2a*−/− and *Epm2b*−/− mice show polyglucosan inclusions (PGs) in muscle, the heart, and brain by the age of 2 months. Later on, behavioral alterations begin with slight motor coordination and activity impairment, abnormal postures of hindlimbs, memory defects, and epileptiform activity from 4 to 9 months. The phenotype significantly worsens over time being spontaneous myoclonic seizures evident from 9 months of age [12, 15, 16]. Intriguingly, it has been reported an opposite phenotype comprising enhanced excitability [12] and accumulated activity [16] in 4-month-old *Epm2a*−/− mice, and hyperactivity and increased exploratory behavior in 11-month-old *Epm2b*−/− mice [17]. Hence, it should be borne in mind that different phenotypical presentations might be determined by age or strain background in LD mice.

Lack of laforin or malin in mice has been related not only to defects in glycogen homeostasis but to defects in protein clearance systems such as autophagy [15, 18] and proteostasis [19, 20], mitochondrial dysfunction [21, 22], and oxidative stress [23]. Furthermore, LD mouse models show neurodegeneration [17, 24] and astrogliosis with reactive astrocytes accumulating the bulk of polyglucosan inclusions [25, 26]. In connection to reactive astrocytes, an early and progressive neuroinflammatory status was tracked in the brain of LD mice from 3 to 16 months of age [27], unraveling neuroinflammation as a common feature in neurodegenerative diseases [28]. Related to neuronal function, alterations in excitatory glutamatergic [29, 30] and inhibitory GABAergic transmissions [31] were described which might account for the increased synaptic excitability [17], the propensity to myoclonic seizures, and sensitivity to convulsant agents observed in LD mouse models [32, 33].

Even though the pathophysiological mechanism in LD is not deciphered yet, LD mouse models have become a useful tool to conduct preclinical studies since they reproduce similar symptoms as in human patients. In this regard, our previous work validated metformin, an oral antidiabetic drug, as an effective therapeutic in *Epm2b*−/− mice [24, 34]. This work led us to obtain the designation of metformin as an orphan drug by the European Medicines Agency (EMA) and the USA Food and Drug Administration (FDA) for the treatment of Lafora disease. Recently, it has been reported an 18-month treatment with metformin in ten patients at the middle/late stages of LD. This study was not conclusive in terms of the beneficial effects of the drug but suggested that treatments should be attempted as early as possible in the course of LD [35]. On the other hand, a therapeutic strategy based on a fusion of human pancreatic α-amylase to a cell-penetrating antibody fragment (VAL-0417), dramatically reduced LBs loads after 8-day intracerebroventricular infusion in *Epm2a*−/− mice [36]. Despite its effectiveness, the application of this approach in human patients is still under revision, and the clinical application has not been initiated yet.

While the assessment of new possible treatments of LD is in course, our approach is to look for novel repurposing drugs which could be beneficial in LD since their translation to the clinic would be straightforward. Neuroinflammation seems to be an important and early trait in LD mouse models [27], thus we decided to assess the possible beneficial effects of two compounds previously used as neuroinflammatory-modifying therapies in other neurological disorders. The selected compounds were propranolol, a β-adrenergic antagonist, and epigallocatechin gallate (EGCG), an antioxidant compound present in green tea extract. Propranolol is also able to ameliorate microglial reactivity [37, 38], and perhaps this is the reason for his recognized anti-neuroinflammatory [39, 40] and neuroprotective properties [41], although its molecular mechanism is still unknown. EGCG has also been used in diseases with a neurological base to counteract neuroinflammation [42–44]. In this work, we have administered these compounds to 3-month-old *Epm2b*−/− mice (corresponding to early stages of LD) for 2 months. We have analyzed motor (motor coordination, beam balance, and abnormal postures) and cognitive tasks (memory and depressive-like behavior) in these mice, as well as histopathological determinants in the brain [presence of polyglucosan inclusions (PGs), neuronal mass, and neuroinflammation markers] to evaluate the effectiveness of both pharmacological interventions. We found an improvement in some behavior tests and some histopathological parameters related to neuroinflammation, especially in the case of propranolol, confirming the potential therapeutic effects of this compound in LD.

Material and Methods

Animals

Malin knockout mice (*Epm2b*−/−) [15] were obtained on a pure B6 background by backcrossing more than 10 generations with corresponding C57BL/6JRccHsd mice (WT) from Harlan laboratories. Mice were maintained at the IBV-CSIC facility on a 12 light/dark cycle with food and water ad libitum. A total of 21 WT and 33 *Epm2b*−/− male mice were randomly assigned to three groups (untreated, propranolol, and EGCG treated; WT $N = 7$ and *Epm2b*−/− $N = 11$ for each group). Although no sex-link phenotype has been reported in mice or humans for Lafora disease, we utilized male mice to compare the results with previous data obtained in the lab.

Drugs and Administration

A racemic mixture of (±)-propranolol hydrochloride (#P0884) and (−)-EGCG (#E4268) were obtained from Sigma-Aldrich. Animals of 3 months of age were treated with either vehicle (saline solution), propranolol (10 mg/Kg), or EGCG (20 mg/Kg) by intraperitoneal administration in a volume of 100 μl, three times per week, during 2 months. Drug doses were based on a bibliographic search for both propranolol [38, 45] and EGCG [43]. These studies concluded that the doses we used in our study were safe and that both compounds reached the brain to exert their effects.

Behavioral Tests

After a 2-month treatment, animals were subjected to a battery of behavioral tests conducted during the light phase from 8:00 a.m. to 3:00 p.m. The order of the behavioral tests and resting time between them were the same for each mouse. The battery of behavioral tests consisted of five tests performed in the following order: hindlimb clasping, beam balance, pole test, Y-maze spontaneous alternation, object location memory, and tail suspension test (see Supplementary Fig. S1). Tests were conducted in order of increasing invasiveness: motor, memory, and depression. Mice rested 48–72 h between tests.

- Hindlimb clasping: Hindlimb clasping scores abnormal postures related to neurodegeneration and has been used as a marker of disease progression in a large number of neurodegenerative mouse models [46]. Mice were grasped by their tail for 10 s and hindlimb position were scored from 0 to 2 [47]. If the hindlimbs were consistently splayed outward, away from the abdomen, it was assigned a score of 0. If one hindlimb was retracted toward the abdomen, it received a score of 1. If both hindlimbs were retracted toward the abdomen it received a score of 2.
- Beam balance: Beam balance assesses fine motor coordination and balance in mice [48]. We analyzed the time taken to cross three beams of 26-,12-, and 5-mm width, 100 cm in length, and 50 cm in height above the floor. Training on day 1 and test on day 3 consisted of crossing three times each beam consecutively with an inter-trail interval (ITI) of 10 min between beams.
- Pole test: The pole test was used to assess basal ganglia-related movement disorders in mice [49, 50]. Mice were placed head upward on the top of a vertical pole (55 cm in length and 8 mm in diameter) and the time is taken to turn completely down, and the time to climb down the pole or descend into the cage was measured. Training on day 1 and test on day 4 consisted of performing the pole test five times consecutively.
- Y-maze: This task probes non-hippocampal short-term working memory [51]. Mice were placed in the center of a Y maze and were allowed to explore the three arms of the maze freely for 5 min. An entry was counted when all four limbs were within the arm. A complete or incomplete arm entry was differentiated based on whether mice reach up to the end of the arm, or just to the middle of the arm, respectively. A correct spontaneous alternation was considered as the entry into three different arms consecutively. Finally, % spontaneous alternation was determined by dividing the number of alternations by the total number of possible alternations (the total number of arm entries minus 2) and multiplying by 100. Mice with less than 6 arm entries during the 5-min single trial were excluded from the analysis.
- Object location memory (OLM): Object location memory probes spatial recognition memory depending on the hippocampus. This task was performed in three phases of habituation, training, and test [52]. Mice were habituated to an empty area for 10 min 24 h before training. In the training phase, two identical objects (familiar) were placed in the arena, and the mouse was allowed to explore them for 5 min. To assess short-term memory, the test was conducted 90 min after training. In the test phase, one of the familiar objects was moved to a different location (novel), and then the mouse explored them again for 5 min. Time exploring both novel and familiar objects was measured, and the discrimination index (DI) was calculated as follows: (time exploring the novel object − time exploring the familiar) / (time exploring novel + familiar) × 100. DI was used as a measure of the recognition of novel location and location memory. Furthermore, the exploratory time was also represented as a measure of attention [53]. Animals that did not explore more than 3 s total for both objects during testing were excluded from the analysis.
- Tail suspension test (TST): TST was developed as a rodent screening test for potential human antidepressant drugs [54]. To assess depressive-like behavior, mice were suspended by their tail for 6 min in an inescapable but moderately stressful situation. The lack of scape-oriented movements is considered immobility. The first time to surrender and total immobility time were measured as indicators of latency to defeat and despair against a stressful situation, respectively [55].

Tissue Collection

After resting for 48 h from the last behavioral test (TST), animals were euthanized by cervical dislocation, and brains were removed. The left hemisphere was quickly dissected into 3 pieces (cerebellum, cortex-hippocampus, and the rest of the

brain), immediately frozen in liquid nitrogen, and preserved at − 80 °C for further use. The right hemisphere was immediately fixed in 4% paraformaldehyde (PAF) at 4 °C overnight and embedded in paraffin for histological analysis.

RNA Extraction and RT-qPCR Analysis

RNA extraction and RT-qPCR analyses were performed in frozen cortex-hippocampus samples as in [27]. The β-actin (Actβ) gene was used as the endogenous reference control to normalize target gene expression. The primers used were: CXCL10-forward 5′–CCGTCATTTTCTGCCTCATC-3′, CXCL10-reverse 5′–CTCGCAGGGATGATTTCAAG-3′, Actβ–forward 5′- ACTGAGCTGCGTTTTACACC-3′ and Actβ–reverse 5′- AGCCATGCCAATGTTGTCTC-3′.

Histopathological Analysis

Five-micrometer paraffin sagittal sections were obtained by microtome and before histological staining, sections were deparaffinized and hydrated with deionized water.

The detection of PGs was performed by periodic acid Schiff (PAS) staining (Sigma), following the manufacturer recommendations. After staining, sections were dehydrated and mounted in depex-based mounting media (Merck Millipore) (Fig. S2).

For immunohistochemical analysis, after rehydration, three steps of antigen retrieval, autofluorescence quenching, and blocking of non-specific staining were performed as follows. For heat antigen retrieval, brain sections in citrate buffer (10 mM, pH = 6) were intermittently boiled in the microwave for 6 s, with a 24-s interval without heating, for 10 min. For autofluorescence quenching, sections were immersed in 1 mg/ml sodium borate for 40 min. For blocking of non-specific staining, sections were incubated with blocking buffer (10% fetal bovine serum, 1% bovine serum albumin, 0.2% Triton X-100) for 1 h at room temperature. Next, sections were incubated with primary antibodies: rabbit anti-NeuN (1:500, Millipore #ABN78), mouse anti-glial fibrillary acidic protein (GFAP) (1:500, Sigma #G3893), guinea pig anti-GFAP (1:500, Synaptic Systems #173_004), rabbit anti-Iba1 (1:100, WAKO #019–19,741), and mouse anti-IP10/CXCL10 (1:20, Abcam #ab8098). All primary antibodies were incubated at 4 °C overnight. After 1× phosphate-buffered saline washing, they were incubated at room temperature for 45 min with the corresponding Alexa Fluor-conjugates [1:500, Life Technologies: goat anti-rabbit IgG Alexa Fluor® 488 (#A11008) or 633 (#A21071), goat anti-mouse IgG Alexa Fluor® 488 (#A11029) or 633 (#A21050), and goat anti-guinea pig IgG Alexa Fluor® 594 (#A11076)]. Background controls of secondary antibodies were performed in parallel. Nuclear staining was performed with DAPI (Sigma). Coverslips were mounted with Fluoromount-G™ (Invitrogen by Thermo Fisher Scientific) (see Supplementary Fig. S2).

Image Acquisition and Analysis

To ensure accurate counts throughout the brain, two sections per animal with a 24-μm-gap between them were selected, stained, and analyzed. For every brain section, three pictures were taken in different hippocampal areas: Cornus Ammonis (CA1), molecular layer of CA1 plus DG (CA1-DG), and dentate gyrus (DG) (see Supplementary Fig. S2). In total, 6 pictures were quantified and averaged per animal. PAS-staining photomicrographs were acquired using a Leica DM RXA2 microscope (Nussloch, Germany) connected to a Hamamatsu color camera (Tokyo, Japan) with an × 40 magnification in RGB format. Immunofluorescence images were acquired using a Leica TCS Sp8 laser-scanning confocal microscope with an × 40 objective. 10–12 *z*-axis stacks separated by 0.33 μm were taken per section, and 2D reconstruction was projected as maximum intensity using ImageJ software (NIH, Bethesda, MD, USA). For automated computer image analysis, we programmed tailored macros in ImageJ for each histological detection. RGB images from PAS staining (see Supplementary Fig. S3A) were firstly split using color deconvolution macro within ImageJ. Next, the red channel was thresholded and finally, an analysis of particles > 0.60 μm^2 applied. The data window lists the count or number of particles, % of the total area occupied by them, and the average size. On the other hand, fluorescence images from NeuN (see Supplementary Fig. S3B), and CXCL10, GFAP, and Iba1 (see Supplementary Fig. S3C) were first thresholded and % occupied area measured. In addition, the NeuN threshold was saturated, and the thickness of the granular cell layer (GCL) was quantified (see Supplementary Fig. S3B), measuring for every pixel the length of the GCL along the *y*-direction and averaging the whole thickness.

Data Analysis

Statistical analysis was performed with RStudio R-3.4.2 [56]. Quantitative data were represented as mean ± standard error of the mean (SEM) with a 95% confidence interval. The normality of the data was analyzed by the Shapiro-Wilk test and homogeneity of variance by the Levene test. To assess the statistical significance (p value) of the effects in multiple comparisons, data with a normal distribution were analyzed by two-way ANOVA followed by a Tukey's post hoc test. Non-parametric data were analyzed by Kruskal-Wallis followed by Dunn's test. To assess the effect size of the interventions in multiple comparisons, Cohen's delta coefficient (d) was calculated and scored as negligible ($d < 0.20$), small ($d \geq 0.20$), medium ($d \geq 0.50$), large ($d \geq 0.80$), and much larger ($d \geq 1.00$) size effect [57, 58]. A descriptive and inferential statistical summary of analyzed behavioral and histopathological variables is supplied (see Supplementary Table S1). Correlation analysis between quantitative variables was

performed using Pearson's method, where the correlation coefficient (r) and p value were calculated and scored as small ($r \geq 0.10$), medium ($r \geq 0.30$), large ($r \geq 0.50$), and much larger ($r \geq 0.70$) [57, 58]. A critical value for significance of $^{*}p < 0.05$ was used throughout the study.

Results

In this work, we have evaluated the efficacy of the treatment of *Epm2b*−/− mice with propranolol and EGCG, two compounds previously used as neuroinflammatory-modifying therapeutic agents (see Introduction). Treatments were administered in male mice of 3 months of age (corresponding to an early stage of LD) for 2 months. After treatments, we performed an in vivo analysis of motor and cognitive behavior followed by an ex vivo histopathological analysis of PG inclusions, astrogliosis, microgliosis, and neuronal mass in the corresponding brains.

Neither Motor Phenotype nor Neurodegenerative Signs Were Detected in 5-Month Old *Epm2b*−/− Mice

Motor behavior was analyzed in *Epm2b*−/− mice by evaluating motor ability and abnormal postures related to neurodegeneration. Mice were assessed for fine motor coordination and balance using two motor tests: pole test and beam balance, and for abnormal postures using the hindlimb clasping test. However, no impairments in the performance of any motor test or hindlimb clasping score were detected in *Epm2b*−/− mice compared to WT at 5 months of age (post-treatment) (see Supplementary Table S1). Therefore, motor ability defects and major neurodegenerative signs were not present in *Epm2b*−/− mice at the assayed age.

Some Cognitive Impairments in *Epm2b*−/− Mice Are Improved by Propranolol and EGCG Treatments

The cognitive profile was evaluated in *Epm2b*−/− mice at 5 months of age by assessing working memory, short-term location memory, and depressive-like behavior (Fig. 1). To evaluate working memory, animals were tested for the spontaneous alternation in the Y-maze, and % spontaneous alternations and % incomplete arm entries were quantified (Fig. 1a, b). Regarding % spontaneous alternations (Fig. 1a), we observed no statistically significant differences in means (p value) and no large effect size (d) between untreated control and *Epm2b*−/− mice (see Supplementary Table S1). In light of these results, we concluded that *Epm2b*−/− mice did not display any working memory defect. We only noticed an increase of % spontaneous alternations in propranolol-treated *Epm2b*−/− mice (65.38 ± 3.58) in comparison to untreated *Epm2b*−/− mice (56.76 ± 3.25), with a medium effect size ($d = -0.78$), but with no statistical significance ($p = 0.789$) (Fig. 1a). In contrast, % incomplete arm entries were significantly increased in untreated *Epm2b*−/− (9.77 ± 2.48) compared to WT mice (2.52 ± 1.65, $p = 0.027^{*}$, $d = -1.02$ large) (Fig. 1b), suggesting an attention defect in ending the task. Interestingly, EGCG treatment was capable of decreasing % incomplete arm entries in *Epm2b*−/− mice from 9.77 ± 2.48 to 3.91 ± 1.20, almost significantly ($p = 0.057$) and with a large effect size ($d = 0.89$), suggesting a positive effect of EGCG in improving the staying on-task of exploration.

More related to hippocampal memory, we studied spatial short-term memory using the object location memory test (OLM) (Fig. 1c, d). The discrimination index (DI) of object location and the total object exploratory time were measured. There were no significant differences (p value) or remarkable effect size (d) in DI among all the groups (Fig. 1c; Table S1), suggesting that short-term location memory was not affected in *Epm2b*−/− mice at 5 months of age. However, we were able to detect a tendency to a decrease in total exploratory time in *Emp2b*−/− (15.45 ± 2.95) compared to WT (26.92 ± 4.49, $p = 0.143$, $d = 1.07$ large) in untreated animals (Fig. 1d). These results suggest that a malin deficit was not affecting hippocampal location memory, but a difference in staying on-task of exploration emerged again in *Epm2b*−/− mice. Moreover, we nicely observed that propranolol treatment increased significantly the total exploratory time, reengaging the attention to exploration in *Epm2b*−/− mice (32.10 ± 3.40, $p = 0.003^{**}$, $d = -1.61$ large) (Fig. 1d). In contrast, EGCG had only a minor effect on this parameter (24.06 ± 2.47, $p = 0.314$, $d = -0.96$ large) in these animals (Fig. 1d). In control animals treated with propranolol, we also observed a tendency to an increase in the exploratory time, although it was not statistically significant (see Supplementary Table S1).

Finally, to assess a possible depressive-like behavior, we performed the tail suspension test (TST) (Fig. 1e, f). The total immobility time and the time that is taken to surrender the first time were measured. Untreated *Epm2b*−/− mice showed a tendency to spend less time immobile (59.4 ± 13.1 s) than WT (104.8 ± 10.5 s, $p = 0.253$, $d = 1.18$ large) (Fig. 1e) and took more time to surrender the first time (213.0 ± 29.3 s) than WT (143.1 ± 13.7 s, $p = 0.201$, $d = -0.87$ large) (Fig. 1f). Although results in TST were not statistically significant, they were large in effect size (d), pointing out that *Epm2b*−/− mice might be engaged in escape-directed behaviors for longer periods of time, what would be indicative of a resilient behavior. Both treatments propranolol and EGCG showed a tendency to increase total immobility time but values were neither statistically significant (p value) nor large in effect size (d) (see Supplementary Table S1). However, propranolol was capable

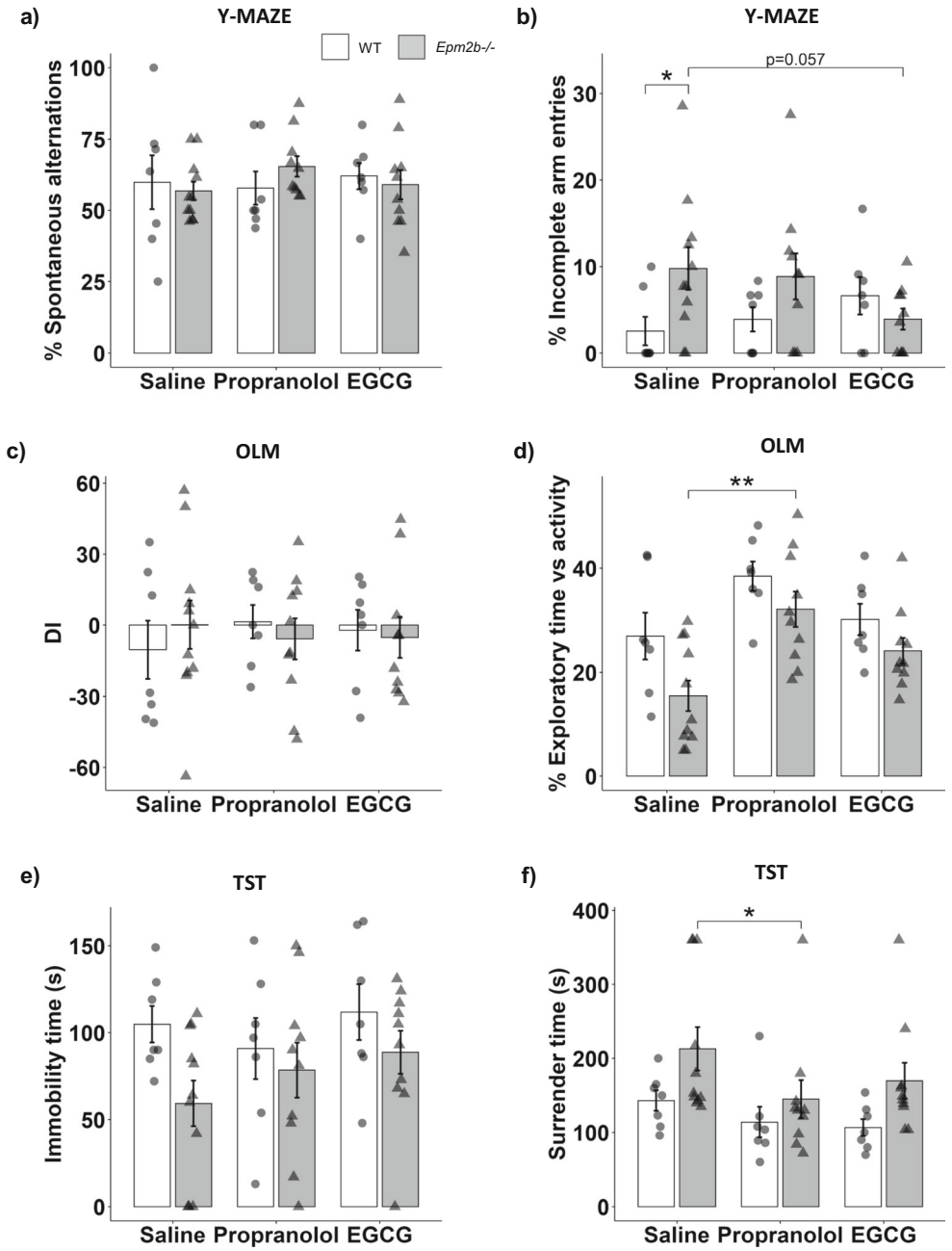

Fig. 1 Cognitive state in *Epm2b−/−* mice and the therapeutic efficacy of propranolol and EGCG treatments. **a**, **b** Evaluation of working memory as measured by Y-maze. **a** % spontaneous alternations represent the measurement of a proper working memory performance; the graph shows mean ± standard error of the mean (SEM) analyzed by two-way ANOVA following a Tukey's posthoc to multiple comparisons. **b** % of the incomplete arm entries showed as means mean ± SEM, analyzed by one-way Kruskal-Wallis following a Dunn's posthoc test to multiple comparisons. **c**, **d** Evaluation of the object location memory test (OLM). **c** Discrimination Index (DI) represents the capability to recognize the change in object location (see Materials and Methods) and **d** % total exploratory time shows the time that mice spent exploring, related to the time they were active. Both graphs indicate mean ± SEM and were statistically analyzed by two-way ANOVA following a Tukey's post hoc to multiple comparisons. **e**, **f** Evaluation of the tail suspension test (TST) for depressive-like behavior evaluation. **e** Total immobility time as mean ± SEM was analyzed by two-way ANOVA following a Tukey's posthoc to multiple comparisons. **f** The first surrender time is represented as mean ± SEM and was analyzed by one-way Kruskal-Wallis following a Dunn's posthoc test to multiple comparisons. Statistical significance was defined as $*p < 0.05$, $**p < 0.01$. WT $N = 7$ and *Epm2b−/−* $N = 11$ for each group. Graph shows individual data points and only those comparisons between groups which were statistically significant. A summary of all descriptive (mean ± SEM) and inferential data (all comparisons between groups) is available in Table S1

of decreasing significantly the latency to surrender the first time in *Epm2b−/−* mice (145.1 ± 25.8 s, $p = 0.016$*, $d =$ 0.75 medium). In contrast, EGCG (169.8 ± 24.3 s, $p = 0.329$, $d = 0.49$ small) had only a minor effect on this parameter.

Propranolol and EGCG Treatments Have Only a Minor Effect on the Formation of Polyglucosan Inclusions in *Epm2b−/−* Mice

Once analyzed the behavioral profile, we collected brain tissues and analyzed them histopathologically. Firstly, brain slices were stained with a periodic acid-Schiff stain (PAS) which detects polyglucosans (PGs). The number of PGs per 10,000 μm^2 and the percentage of the tissue area occupied by them was quantified by image analysis as indicated in the Methods section (see Supplementary Fig. S3). Representative pictures of PAS staining (Fig. 2a) disclosed an enormous amount of PGs in *Epm2b−/−* (99.40 ± 7.05) compared to WT mice (2.89 ± 1.18, $p = 0.0013$**, $d = -4.51$ large) (Fig. 2b), together with a higher percentage of the area occupied by PGs (*Epm2b−/−* 4.61 ± 0.50 vs WT 0.09 ± 0.01, $p = 0.0012$**, $d = -2.98$ large) (Fig. 2c). Treatment of the WT mice with either propranolol or EGCG showed similar values as untreated WT mice (see Supplementary Fig. S4). Despite a smooth trend to a decrease (10–15%) in the number of PGs and the occupied area in propranolol- and EGCG-treated *Epm2b−/−* mice (Fig. 2b, c), the reduction in PGs was not statistically significant (*p* value) or was small in effect size (*d*) (see Supplementary Table S1). Thus, we consider that a 2-month propranolol or EGCG treatments might have, if any, only a minor effect preventing the formation of PG inclusions in *Epm2b−/−* mice.

Propranolol and EGCG Treatments Ameliorate Neuronal Disorganization of the CA1 Layer of the Hippocampus Present in *Epm2b−/−* Mice

In the light of a pervasive presence of PG inclusions in *Epm2b−/−* brain, we next sought to confirm neuronal and/or astrocytic alterations connected with it. In brain slices, we detected the nuclear neuronal marker NeuN, the astrocytic marker GFAP, and the nuclear marker DAPI by immunofluorescence (Fig. 3). In the hippocampus, neuronal bodies were tightly packed in the granular cell layer (GCL), as revealed by the NeuN signal in red and DAPI staining in blue (Fig. 3a). To evaluate neuronal alterations through the hippocampus, we quantified both the NeuN area, as a measurement of neuronal density, and the thickness of the granular cell layer (GCL), as an index of a proper neuronal organization, in three brain areas of the hippocampus: Cornus Ammonis (CA1), molecular layer of CA1 plus DG (CA1-DG), and dentate gyrus (DG) (Fig. S2). We found no significant differences in the overall NeuN area among groups (Fig. 3b, see Supplementary Table S1), suggesting that *Epm2b−/−* mice were not suffering from abnormal densities of granular neurons. However, we found a tendency to thicker overall GCL in untreated *Epm2b−/−* (92.11 ± 3.78 μm) than in WT mice (78.16 ± 5.32 μm, $p = 0.233$, $d = -1.06$ large), highlighting a possible alteration in the anatomical organization of neuronal networks (Fig. 3c). Propranolol treatment (72.63 ± 4.70 μm, $p = 0.0130$*, $d = 1.42$ large) was able to diminish the overall thickness of GCL in *Emp2b−/−* mice down to WT levels (Fig. 3c). In contrast, EGCG was not as effective as propranolol (78.00 ± 3.83 μm, $p = 0.9341$, $d = 1.14$ large). Interestingly, this

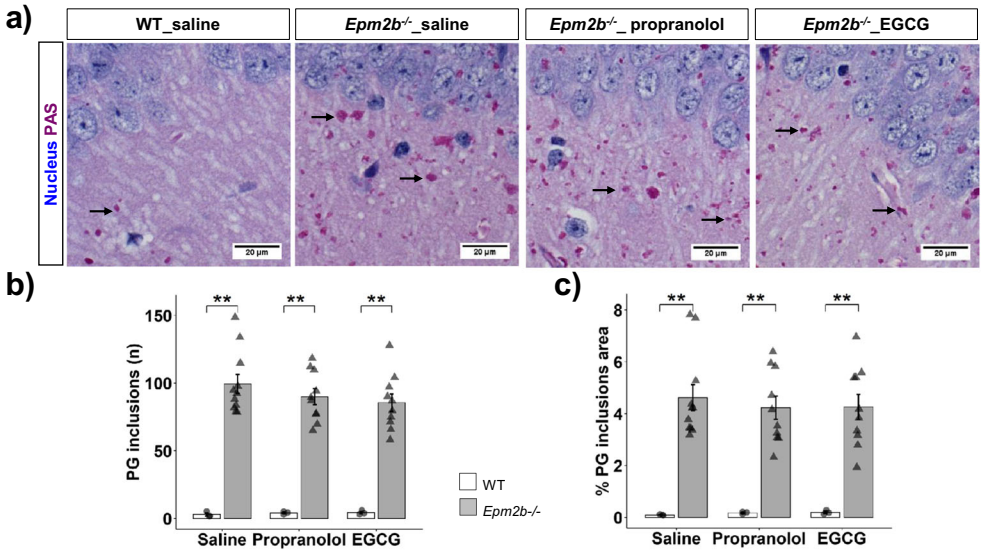

Fig. 2 Accumulation of PGs in the hippocampus as measured by PAS staining. **a** Representative microscopy image of PGs detection (in pink; see also black arrows) in CA1 region of the hippocampus by PAS staining; neural nucleus are in blue. **b**, **c** Bar plots show the number (**b**) and % of the occupied area (**c**) of PGs per 10,000 μm^2. Graphs represent mean ± SEM of three different micrographs from CA1, CA1-DG, and DG regions from two slices for every mouse ($N = 3$ WT and $N = 11$ *Epm2b−/−* for each group of treatment). A one-way Kruskal-Wallis followed by Dunn's test posthoc was run to analyze both the number and the % of the occupied area, **$p < 0.01$. Graph shows individual data points and only those comparisons between groups which were statistically significant. A summary of all descriptive (mean ± SEM) and inferential data (all comparisons between groups) is available in Table S1. Scale 20 μm

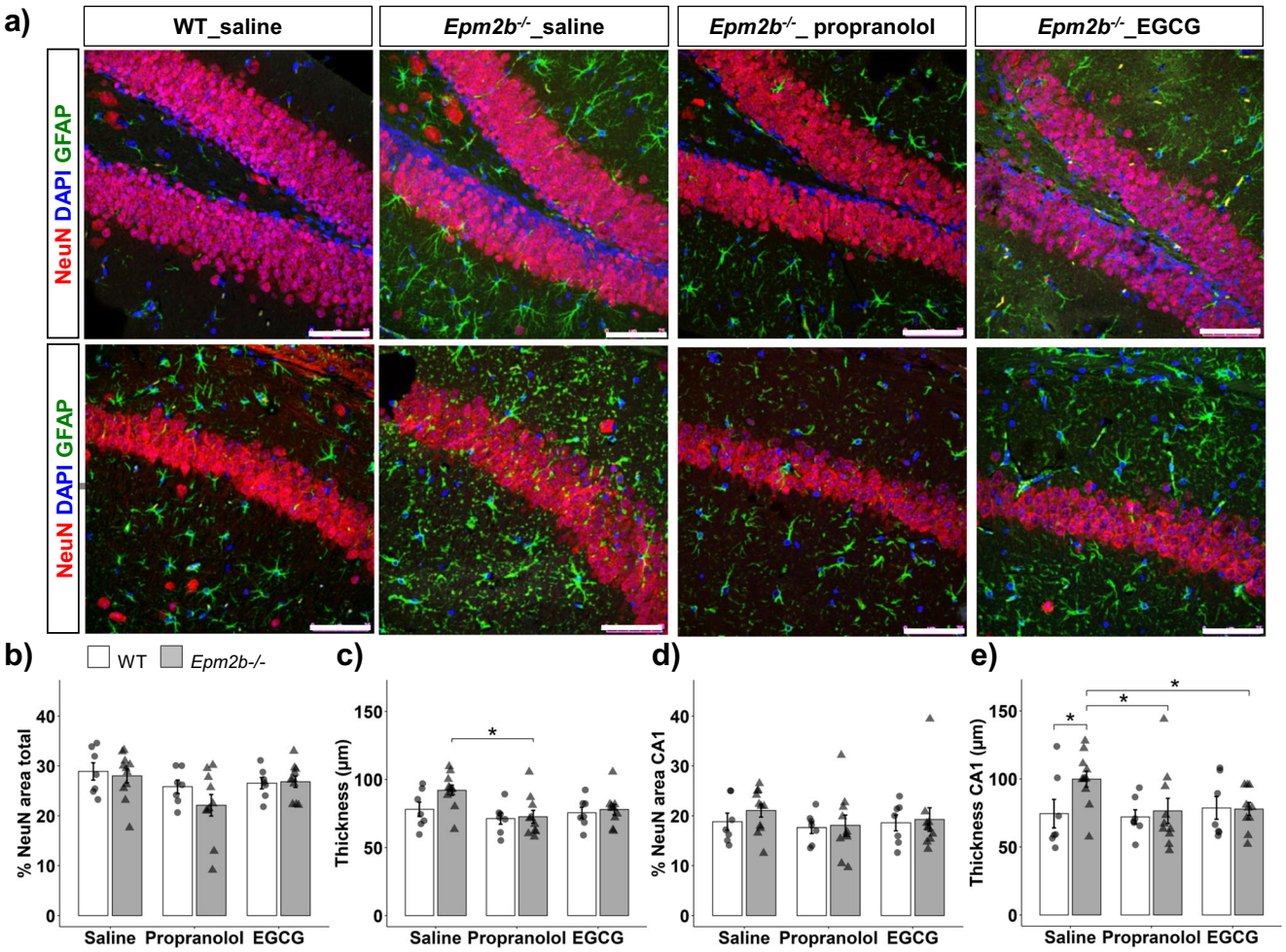

Fig. 3 Neuronal mass and thickness of the granular cell layer. **a** Representative immunofluorescence confocal microscopy image of NeuN (in red) and GFAP (in green) in the dentate gyrus (upper rows) and CA1 (lower rows) areas of the hippocampus; DAPI staining for the nucleus is in blue. **b** Analysis of the % NeuN total area in the hippocampus (DG plus CA1) and **c** average thickness (in microns) of the granular cell layer (GCL) in these areas. **d** Analysis of the % NeuN area of the CA1 region and average thickness (in microns) of the GCL in the CA1 region. **e** Graphs represent mean ± SEM of three different micrographs from the CA1 and DG regions from two slices for every mouse ($N = 7$ WT and $N = 11$ *Epm2b*−/− for each group of treatment). Two-way ANOVA was run to analyze the NeuN area and thickness of DG and CA1 regions following a Tukey's post hoc. A one-way Kruskal Wallis test was run to analyze the NeuN area and thickness of the CA1 region followed by Dunn's test. $p^* < 0.05$. Graph shows individual data points and only those comparisons between groups which were statistically significant. A summary of all descriptive (mean ± SEM) and inferential data (all comparisons between groups) is available in Table S1. Scale 75 µm

neuronal disorganization throughout GCL was more remarkable in the hippocampal CA1 region (Fig. 3d, e). In the CA1 area, although there were no major differences in the NeuN area between untreated *Epm2b*−/− and WT mice (see Supplementary Table S1) (Fig. 3d), there was a significant increase in CA1 thickness in untreated *Epm*2b−/− mice (99.96 ± 5.80 µm) compared to WT mice (74.49 ± 10.44 µm, $p = 0.016^*$, $d = -1.11$ large) (Fig. 3e). Interestingly, both propranolol and EGCG treatments were efficient in reducing thickness in the CA1 region of the *Epm2b*−/− mice (76.53 ± 9.23 µm, $p = 0.014^*$, $d = 0.95$ large and 77.94 ± 4.81 µm, $p = 0.047^*$, $d = 1.26$ large, respectively) down to control levels (Fig. 3e). Treatment of the WT mice with either propranolol or EGCG showed similar values as untreated WT mice (see Supplementary Fig. S4).

In addition to neuronal alterations, and in agreement with previous observations [24, 59], we noticed a remarkable GFAP positive signal (in green) in untreated *Epm2b*−/− mice compared to WT (Fig. 3a) which was deeply studied in the next section of results.

Propranolol Treatment but Not the EGCG One Markedly Reduces Reactive Astrogliosis in *Epm2b*−/− Mice

To gain insight into the astrocytic activation in the hippocampus, we examined reactive astrogliosis and the production of the proinflammatory CXCL10 cytokine in *Epm2b*−/− mice. We detected the astrocytic marker GFAP (in green), the

CXCL10 cytokine (in white), and the nuclear marker DAPI (in blue) by immunofluorescence (Fig. 4a). As described previously [59], untreated *Epm2b−/−* showed an extraordinary GFAP+ area (13.30 ± 1.27) compared to WT mice (6.15 ± 1.03, $p = 0.0013$**, $d = -1.90$ large) (Fig. 4b), suggesting a remarkable pathological reactive astrogliosis in the brain of *Epm2b−/−* mice. We also found higher levels of CXCL10+ area in untreated *Epm2b−/−* (5.29 ± 1.01) compared to WT (1.79 ± 0.74, $p = 0.040$*, $d = -1.19$ large) (Fig. 4c), and the relative expression of CXCL10 mRNA was also higher in *Epm2b−/−* mice (6.31 ± 1.62) than in control animals (1.05 ± 0.13, $p = 0.0154$*, $d = -1.95$ large), in agreement with previous results [27]. Regarding the effectiveness of treatments in preventing reactive astrogliosis, only propranolol but not EGCG decreased the GFAP+ signal in *Epm2b−/−* (8.59 ± 1.22, $p = 0.037$*, $d = 1.16$ large) down to WT levels (Fig. 4b). Unfortunately, neither EGCG nor propranolol treatments modified the presence of CXCL10 in the brain either at the protein or mRNA levels (Fig. 4c, d) (see Supplementary Table S1). Treatment of the WT mice with either propranolol or EGCG showed similar values as untreated WT mice (see Supplementary Fig. S4).

In brain slices, we noticed that CXCL10 expression coincided with reactive GFAP+ astroglia, indicating a pro-inflammatory response of the reactive astroglia in *Epm2b−/−* (Fig. 4a) although not all GFAP+ cells were also CXCL10+. This suggests the existence of two subpopulations of reactive astrocytes (which account for around 13% of total

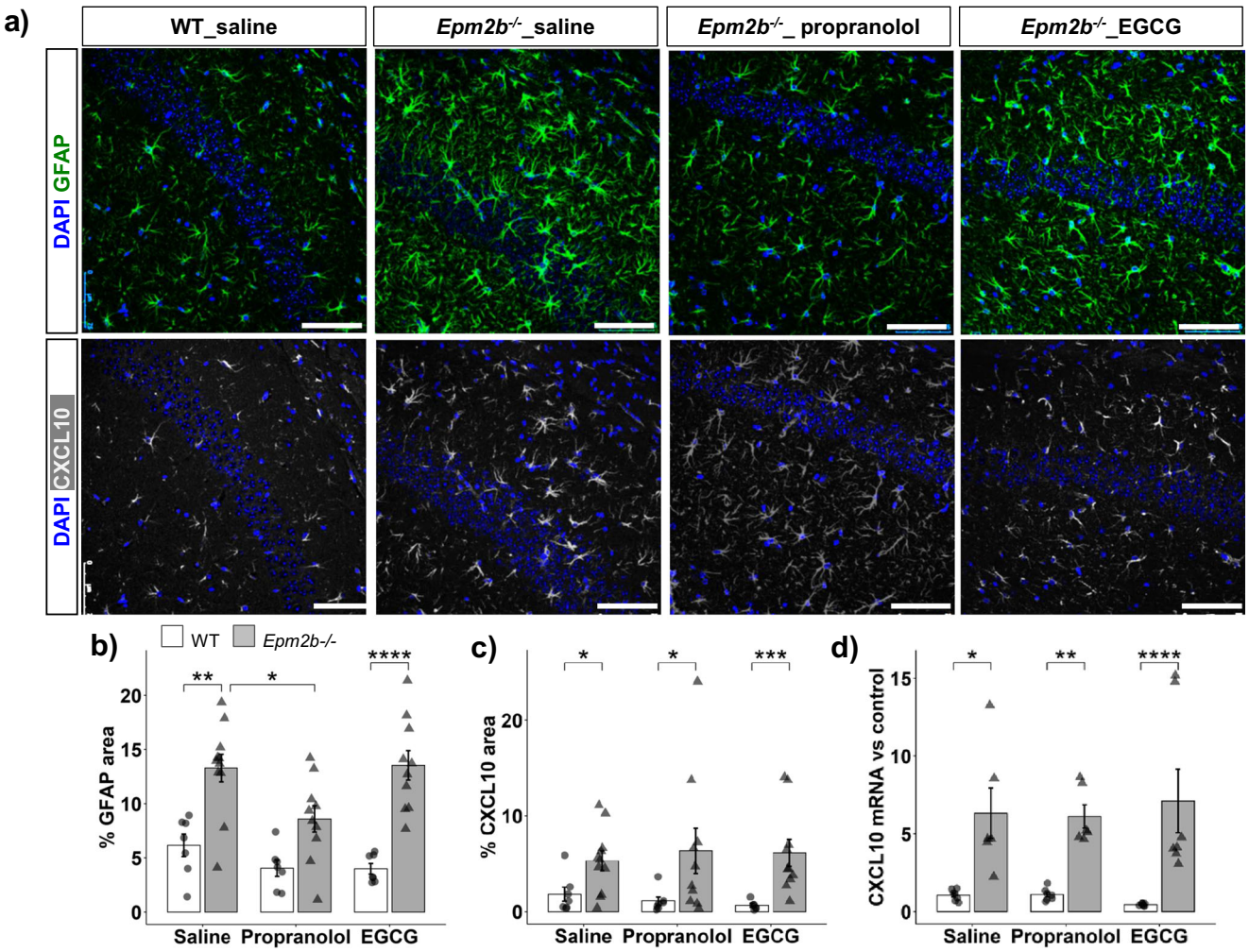

Fig. 4 Reactive astrogliosis and neuroinflammation in *Epm2b−/−* mice. **a** Representative immunofluorescence confocal micrographs for the same area of GFAP (green, upper rows), CXCL10 (white, lower rows), and DAPI staining (blue) of the CA1 region of the hippocampus. **b**, **c** Percentage of the areas occupied by GFAP (**b**) and CXCL10 (**c**) proteins in the brain. Graphs represent mean ± SEM of three different micrographs of the CA1 region from two slices for every mouse ($N = 7$ WT and $N = 11$ *Epm2b−/−*, for each group of treatment). **d** Relative expression of CXCL10 mRNA in brain tissue. Graph represents mean ± SEM of the expression ratio vs WT treated with saline samples ($N = 7$ WT and $N = 7$ *Epm2b−/−*). Two-way ANOVA was run to analyze the % GFAP area following a Tukey's post-hoc. A one-way Kruskal Wallis followed by Dunn's test was run for % CXCL10 area and relative levels of CXCL10 mRNA. *$p < 0.05$, **$p < 0.01$, ***$p < 0.001$, ****$p < 0.0001$. Graph shows individual data points and only those comparisons between groups which were statistically significant. A summary of all descriptive (mean ± SEM) and inferential data (all comparisons between groups) is available in Table S1. Scale 75 μm

area), one being GFAP+/CXCL10+ (around 4% of total area), and the other GFAP+/CXCL10- (around 9% of total area). To discard the participation of microglia in the expression of CXCL10, we colocalized the astrocytic GFAP (in green), the microglial Iba1 (in magenta), and cytokine CXCL10 (in red) markers by immunofluorescence (see Supplementary Fig. S5). We observed, first, that there were independent GFAP and Iba1 signals, differentiating two separated astroglial and microglial populations. Second, we observed a perfect spatial overlapping between GFAP and CXCL10 signals, which was completely absent between Iba1 and CXCL10, stressing the fact that the neural population which overexpresses the CXCL10 proinflammatory cytokine was reactive astroglia but not microglia (see Supplementary Fig. S5).

Only Propranolol Treatment Successfully Prevents Microgliosis in *Epm2b−/−* Mice

Having confirmed that CXCL10 was broadly expressed by reactive astrocytes but not in microglia in *Epm2b−/−* mice, next, we wanted to figure out whether microglia was also affected in these mice. With this aim, we detected the microglial marker Iba1 (in magenta) and the nuclear marker DAPI (in blue) by immunofluorescence (Fig. 5). Even though the Iba1 area or intensity did not show significant differences among groups, we found clear morphological changes in *Epm2b−/−* microglia (Fig. 5a). It has been reported that an indication of microglia activation is when the cell body swells and becomes less defined and ameboid [60]. The number of Iba1+ cells with changes in morphology was counted, and we

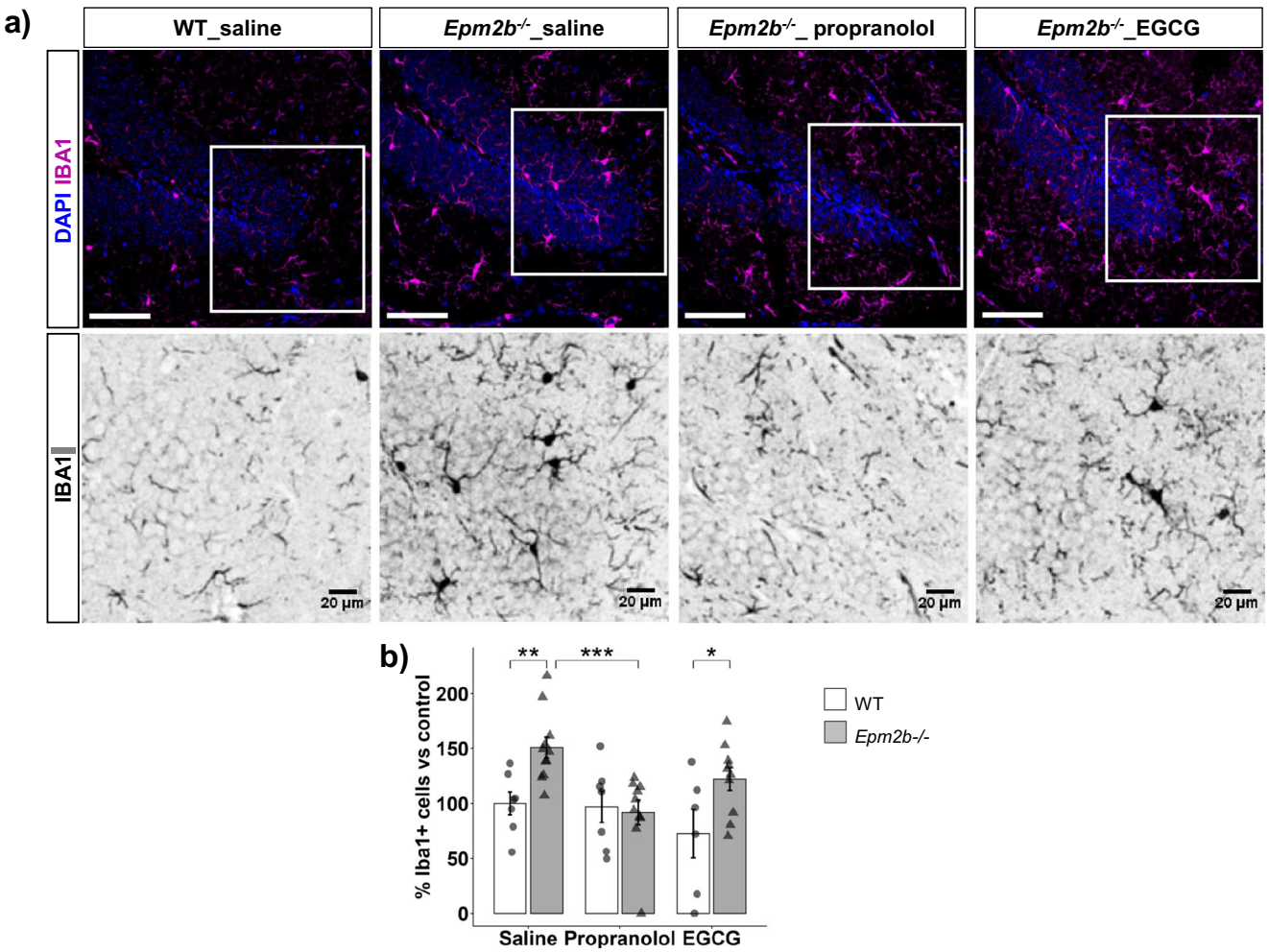

Fig. 5 Reactive microglia in *Epm2b−/−* mice. **a** Representative immunofluorescence confocal micrographs of Iba1 (magenta) and DAPI staining (blue) in the DG of the hippocampus (upper rows), scale 75 µm. In gray (lower rows), amplified images to appreciate the remarkable morphological changes in microglia in *Epm2b−/−* mice; scale 20 µm. **b** % Iba1-positive cells, showing morphological changes in reactive microglia, vs control. The graph represents the mean ± SEM of three different micrographs from the DG area from two slices for every mouse ($N = 7$ WT and $N = 11$ *Epm2b−/−* for each group of treatment). A one-way Kruskal Wallis analysis was run followed by Dunn's test for multiple comparisons. $^{*}p < 0.05$, $^{**}p < 0.01$, $^{***}p < 0.001$. Graph shows individual data points and only those comparisons between groups which were statistically significant. A summary of all descriptive (mean ± SEM) and inferential data (all comparisons between groups) is available in Table S1

observed a significant increase in activated microglia in untreated *Epm2b−/−* (150.0 ± 9.6) compared to WT (100.0 ± 10.4, $p = 0.00507$**, $d = -1.67$ large) (Fig. 5b). Treatment with propranolol decreased the number of altered microglia in *Epm2b−/−* (91.7 ± 11.3, $p = 0.00049$***, $d = 1.75$ large) down to WT levels. In contrast, EGCG treatment was less effective (122.2 ± 10.3, $p = 0.116$, $d = 0.88$ large). Treatment of the WT mice with either propranolol or EGCG showed similar values as untreated WT mice (see Supplementary Fig. S4).

Accumulation of PG Inclusions, Astrogliosis, and Microgliosis Show a Significant Correlation in *Epm2b −/− Mice*

As it is assumed that the accumulation of PGs is causative of LD, we studied whether there was any correlation between the number of PGs and the histopathological findings showed in this work such as neuronal alterations, astrogliosis, or microgliosis (Fig. 6). With this regard, we performed a correlation analysis by Pearson's coefficient determination in RStudio. We found that the analyzed neuronal parameters such as neuronal mass and thickness in the whole hippocampus or in the CA1 area did not correlate with either the levels of PGs, microgliosis, astrogliosis, or CXCL10 levels (Fig. 6). Interestingly, we found a large correlation between the number of PGs and astrogliosis ($r = 0.58$***) and a medium correlation with microgliosis ($r = 0.45$**) and CXCL10 expression ($r = 0.32$*) (Fig. 6). There was also a large correlation between astrogliosis and microgliosis ($r = 0.62$***) as well as between astrogliosis and CXCL10 expression ($r = 0.51$***), and a medium correlation between microgliosis and CXCL10 expression ($r = 0.30$*) (Fig. 6). All these remarkable correlations suggested a close relationship between PGs and these inflammatory processes. In conclusion, we have found that the accumulation of PGs is not linked to defects in neuronal parameters, but to the appearance of reactive astroglia and microglia, which would initiate a pro-inflammatory response.

Discussion

Lafora disease (LD) is a neurological disorder that aggravates with age. Since the first symptoms of LD appear during late childhood or early adolescence [1], in this work, we treated malin-deficient mice (*Epm2b−/−*) at 3 months of age, corresponding with a human age of 20 years [61], for 2 months. The advantage of an early treatment around the onset of the disease is based on targeting a possible still reversible stage of the progression of the disease. At 5-month of age, *Epm2b−/−* mice showed a spread of PG inclusions throughout the brain, especially in the hippocampus, accompanied by extensive microgliosis, reactive astrogliosis, and overexpression of the proinflammatory cytokine CXCL10. This scenario corroborates a neuroinflammatory status at early ages in *Epm2b−/−* mice, as described previously [27]. The large statistical correlation between the presence of PG inclusions and astrogliosis ($r = 0.58$***) might illustrate a likely causative role of PGs for the presence of reactive astrocytes, what it was not surprising, since astrocytes are the main neural type accumulating PGs in the brain [25, 26]. Similarly, the strong correlation between astrogliosis and microgliosis ($r = 0.62$***) provides a clue that somehow reactive astrocytes might be activating microglia within CNS or vice versa; microglia may be the initial point to enhance an inflammatory environment by triggering astrocyte reactivity and making them proinflammatory. Despite the upregulated neuroinflammation, *Epm2b −/−* mice were not losing neurons at 5 months of age, but they presented a remarkable disorganization of the GCL thickness, especially in the hippocampal CA1 region, what is suggestive of an altered neuronal function. These neuronal findings are in the same light as the recently reported abnormalities in dendritic spines of CA1 pyramidal neurons of LD mouse models [62]. However, we found no correlation between neuronal alterations and the presence of PGs or neuroinflammatory markers (Fig. 6), suggesting an independent development of these alterations.

In terms of behavioral and cognitive status, at 5 months of age, and in agreement with other authors [17], we did not observe any affected motor ability in *Epm2b−/−* mice by beam balance, pole test, and hindlimb clasping. However, at this age, *Epm2b−/−* mice displayed a reduction in attention to ending a task, as demonstrated by an increase in the number of incomplete entries in the Y-maze test, and also a reduction in the exploratory time in the OLM test, despite no significant short-term location or working memory defects. Perhaps, the observed disorganization of GCL in the CA1 region could be the cause of the differences in exploratory behavior and attention present in *Epm2b−/−* mice. However, we found that after 2 months of treatment with propranolol and EGCG, there was a complete restoration of the GCL disorganization in the CA1 region in *Epm2b−/−* mice, and this correlated with an improvement in their exploratory behavior and attention. In fact, the restoration of the cytoarchitecture of regions CA1 and CA2 has already been proven as essential to improving cognitive performance during aging [63]. The fact that both propranolol and EGCG restored the disorganization of the CA1 region but only propranolol had a beneficial effect of astroglia and microglia reactivity might suggest a particularly positive effect of EGCG on neuronal function (e.g., antioxidant), but more work would be needed to understand this positive effect.

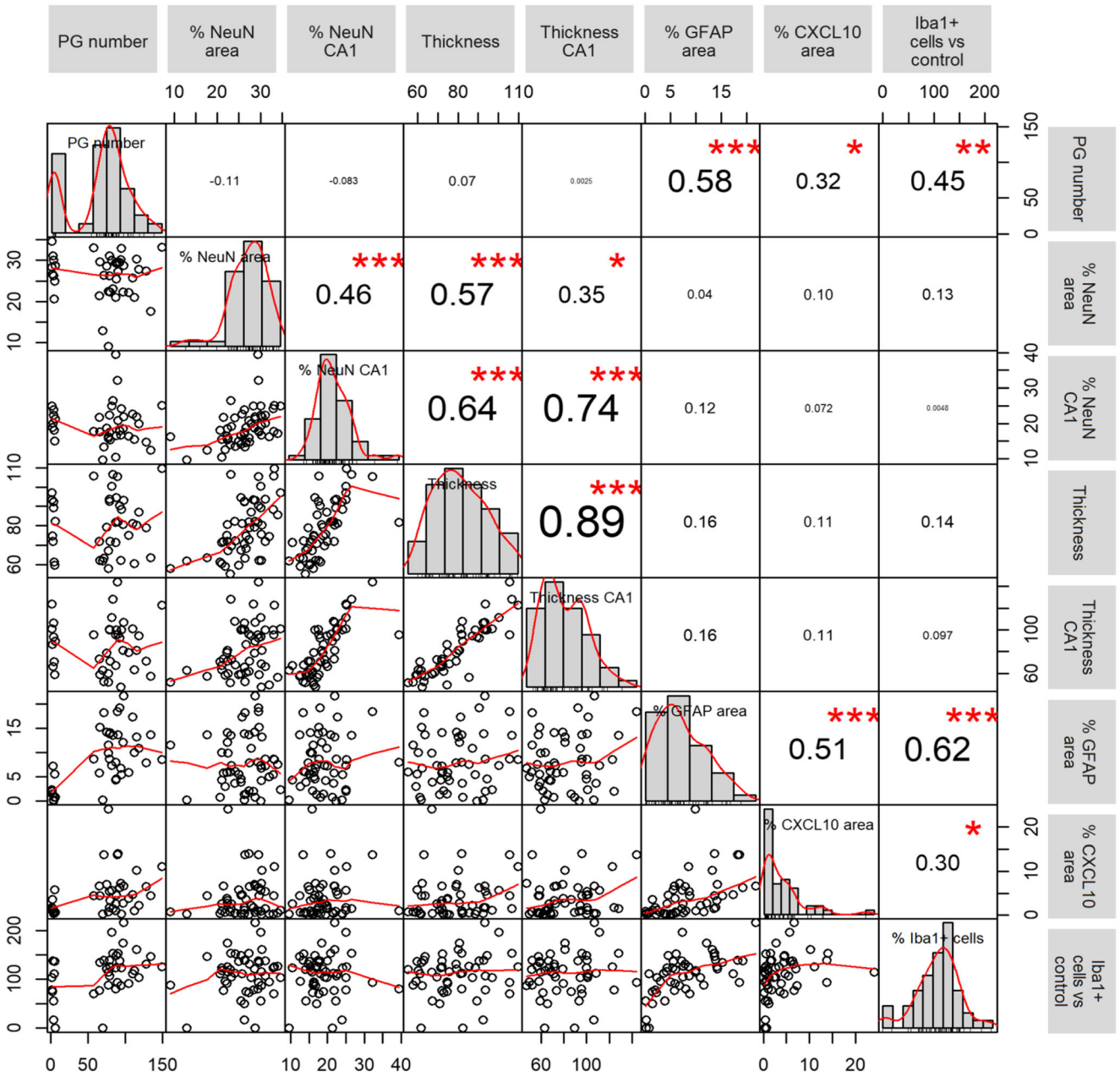

Fig. 6 Correlation matrix between brain pathological markers. The correlation matrix displays the distribution of each variable on the diagonal, the bivariate scatter plots on the bottom, and Pearson's coefficient (r) plus the significance levels (p value) on the top of the diagonal. Pearson's coefficient (r) indicates the direction and the strength of the relationship between the variables. A negative correlation index means an inverse correlation: one parameter increases but the other decreases and vice versa. The strength of the correlation is scored as small ($r \geq 0.10$), medium ($r \geq 0.30$), large ($r \geq 0.50$), and much larger ($r \geq 0.70$) [57]. Significance levels (p value) for correlations: $^{*}p < 0.05$, $^{**}p < 0.01$, $^{***}p < 0.001$

In the TST test, we found a decreased immobility time and an increased latency to defeat in *Epm2b*−/− mice in comparison to WT, which could be interpreted as increased resilience against stress [55, 64], but also as an enhanced reactivity to moderate stress [55]. These results are compatible with a phenotype of hyperactivity and non-anxiety described previously in *Epm2b*−/− mice by other authors [17]. Interestingly, propranolol and EGCG treatments normalized the performance of the *Epm2b*−/− mice in this test, although the effect of propranolol was more effective than EGCG.

Both treatments had only a minor effect, if any, on the formation of PGs in *Epm2b*−/− mice, perhaps because both propranolol and EGCG have no reported action of glycogen synthesis. However, treatment with propranolol decreased the presence of reactive microglia and also prevented the appearance of reactive astrocytes. EGCG treatment had only a minor effect in reducing

Table 1 Pathological features of *Epm2b−/−* mice and the relevance of propranolol and EGCG treatments. The change in means is expressed as no modified, increased, or decreased. A pair of statistical significance (*p* value) and the effect size (*d*) of changes are detailed from posthoc of multiple comparisons and delta Cohen's coefficient, respectively. Significance levels (*p* value): $*p < 0.05$, $**p < 0.01$, and $***p < 0.001$. No significance levels (*p* value): ns. Effect size (*d*): negligible ($d < 0.20$), small ($d \geq 0.20$), medium ($d \geq 0.50$), large ($d \geq 0.80$), and much larger ($d \geq 1.00$) size effect [57, 58]. The parameters with $*p < 0.05$ and *d* large are highlighted in pink and green

Behavioral or histological pathological features	*Epm2b−/−* vs control	*Epm2b−/−*_propranolol vs Epm2b−/−	*Epm2b−/−*_EGCG vs Epm2b−/−
Incomplete exploration behavior	Increased	No modified	Decreased
y-maze: % incomplete arm entries	*p**/*d* large	ns/*d* negligible	*p*=0.057/*d* large
Attention	Decreased	Increased[a]	Increased
OLM: % exploratory time	ns/*d* large	*p***/*d* large	ns/*d* large
Hyperreactivity to stress	Increased	Decreased[a]	Decreased[a]
TST: latency to surrender (time)	ns/*d* large	*p**/*d* medium	ns/*d* small
PG inclusions	Increased	Decreased	Decreased
Number	*p***/*d* large	ns/*d* small	ns/*d* medium
Neuronal disorganization	Increased	Decreased	Decreased
Thickness CA1 (μm)	*p**/*d* large	*p*/d large*	*p**/*d* large
Astrogliosis	Increased	Decreased[a]	No modified
% GFAP area	*p***/*d* large	*p**/*d* large	ns/*d* negligible
Proinflammatory cytokine	Increased	No modified	No modified
% CXCL10 area	*p**/*d* large	ns/*d* negligible	ns/*d* negligible
Microgliosis	Increased	Decreased	Decreased[a]
% Iba1+ cells vs control	*p***/*d* large	*p****/*d* large	ns/*d* large

[a] Similar effect of the treatment was observed in WT mice but without statistical significance

reactive microglia. Perhaps differences in the anti-inflammatory mechanism triggered by propranolol and EGCG could be the explanation for their distinct performance. In this sense, it is known that the anti-inflammatory effects of EGCG are mediated by indirect mechanisms such as reducing reactive oxygen species and reducing NF-kB activity [42], whereas β-adrenergic receptors regulate directly microgliosis [37] and astrogliosis [65]; and propranolol, through the blockage of the β-adrenergic receptors, is effective reducing reactive glia after a wide variety of neuronal insults [38–40]. What it was more intriguing was that propranolol halted reactive astrogliosis but did not modify CXCL10 expression in astrocytes. According to our results, CXCL10 is being expressed in just 4% of the area from a total of 13% of the GFAP+ area in *Epm2b−/−* mice. Thus, it could be possible that propranolol prevented the initial switch from resting to reactive astrocytic population (GFAP+/CXCL10-) without affecting the reactive and proinflammatory population (GFAP+/CXCL10+) of astrocytes already present at the beginning of the treatment (3-month-old mice). This suggests that propranolol would be more effective at the initial stages of the disease before astrocytes become far more proinflammatory.

In summary, the treatment of *Epm2b−/−* mice with propranolol and EGCG during 2 months shows some ameliorating effects in these mice, being propranolol more effective than EGCG (Table 1). These compounds had a minor effect, if any, in preventing the formation of PGs, so the ameliorating effects of these compounds on the behavioral tests must depend on the decrease in the formation of reactive astrocytes and microglia, rather than on their action on the formation of PGs. Thus, our results confirm the potential therapeutic effects of modulators of inflammation as novel treatments in the early stages of Lafora disease. We propose, then, the use of an anti-neuroinflammatory strategy at the early stages of the disease, either alone or in combination with PG-modifying treatments to boost a possible synergistic effect. However, we have to bear in mind that the use of general anti-inflammatory drugs is not recommended because of their detrimental performance in long-term treatments. For this reason, only specific anti-inflammatory compounds whose selection should be made after a deep understanding of the main inflammatory pathways related to LD should be used.

Supplementary Information The online version contains supplementary material available at https://doi.org/10.1007/s12035-021-02285-1.

Authors' Contributions MH and BM performed all experiments. BM analyzed and interpreted the data and was a major contributor in writing the manuscript. PS interpreted the data and wrote the manuscript. All authors have read and approved the final manuscript.

Funding This work was supported by a grant from the Spanish Ministry of Science and Innovation SAF2017-83151-R and a grant from the National Institutes of Health P01 NS097197, which established the Lafora Epilepsy Cure Initiative (LECI), to P.S.

Data Availability All data generated or analyzed during this study are included in this published article and its supplementary information files.

Compliance with Ethical Standards

Competing Interests The authors declare that they have no competing interests.

Ethics Approval and Consent to Participate All animal experiments were approved by the animal committee of the Instituto de Biomedicina de Valencia-CSIC [Permit Number: INTRA12 (IBV-4)] and carried out in accordance with recommendations for the Care and Use of Laboratory Animals of the Consejo Superior de Investigaciones Cientificas (CSIC, Spain).

Consent to Participate Not applicable.

Consent for Publication Not applicable.

Code Availability Not applicable

References

1. Turnbull J, Tiberia E, Striano P, Genton P, Carpenter S, Ackerley CA et al (2016) Lafora disease. Epileptic Disord 18(S2):38–62
2. Sakai M, Austin J, Witmer F, Trueb L (1970) Studies in myoclonus epilepsy (Lafora body form). II. Polyglucosans in the systemic deposits of myoclonus epilepsy and in corpora amylacea. Neurology 20(2):160–176
3. Lafora GR, Glueck B (1911) Beitrag zur histogpathologie der myoklonischen epilepsie. Gesamte Neurol Psychiatr 6:1–14
4. Minassian BA, Lee Jeffrey R, Herbrick JA, Huizenga J, Soder S, Mungall AJ et al (1998) Mutations in a gene encoding a novel protein tyrosine phosphatase cause progressive myoclonus epilepsy. Nat Genet 20(2):171–174
5. Serratosa JM, Gómez-Garre P, Gallardo ME, Anta B (1999) Beltrán-Valero De Bernabé D, Lindhout D, et al. A novel protein tyrosine phosphatase gene is mutated in progressive myoclonus epilepsy of the Lafora type (EPM2). Hum Mol Genet 8(2):345–352
6. Chan EM, Young EJ, Ianzano L, Munteanu I, Zhao X, Christopoulos CC, Avanzini G, Elia M et al (2003) Mutations in NHLRC1 cause progressive myoclonus epilepsy. Nat Genet 35(2): 125–127
7. Gentry MS, Worby CA, Dixon JE (2005) Insights into Lafora disease: Malin is an E3 ubiquitin ligase that ubiquitinates and promotes the degradation of laforin. Proc Natl Acad Sci U S A 102(24):8501–8506
8. Lohi H, Ianzano L, Zhao XC, Chan EM, Turnbull J, Scherer SW, Ackerley CA, Minassian BA (2005) Novel glycogen synthase kinase 3 and ubiquitination pathways in progressive myoclonus epilepsy. Hum Mol Genet 14(18):2727–2736
9. Solaz-Fuster MC, Gimeno-Alcañiz JV, Ros S, Fernandez-Sanchez ME, Garcia-Fojeda B, Garcia OC, Vilchez D, Dominguez J et al (2008) Regulation of glycogen synthesis by the laforin - Malin complex is modulated by the AMP-activated protein kinase pathway. Hum Mol Genet 17(5):667–678
10. García-Gimeno M, Knecht E, Sanz P (2018) Lafora disease: a ubiquitination-related pathology. Cells 7(8):87
11. Nitschke F, Ahonen SJ, Nitschke S, Mitra S, Minassian BA (2018) Lafora disease — from pathogenesis to treatment strategies. Nat Rev Neurol 14(10):606–617
12. Ganesh S, Delgado-Escueta AV, Sakamoto T, Avila MR, Machado-Salas J, Hoshii Y, Akagi T, Gomi H et al (2002) Targeted disruption of the Epm2a gene causes formation of Lafora inclusion bodies, neurodegeneration, ataxia, myoclonus epilepsy and impaired behavioral response in mice. Hum Mol Genet 11(11):1251–1262
13. DePaoli-Roach AA, Tagliabracci VS, Segvich DM, Meyer CM, Irimia JM, Roach PJ (2010) Genetic depletion of the malin E3 ubiquitin ligase in mice leads to Lafora bodies and the accumulation of insoluble laforin. J Biol Chem 285(33):25372–25381
14. Turnbull J, Wang P, Girard JM, Ruggieri A, Wang TJ, Draginov AG, Kameka AP, Pencea N et al (2010) Glycogen hyperphosphorylation underlies Lafora body formation. Ann Neurol 68(6):925–933
15. Criado O, Aguado C, Gayarre J, Duran-Trio L, Garcia-Cabrero AM, Vernia S, San Millán B, Heredia M et al (2012) Lafora bodies and neurological defects in malin-deficient mice correlate with impaired autophagy. Hum Mol Genet 21(7):1521–1533
16. García-Cabrero AM, Marinas A, Guerrero R, Rodríguez De Córdoba S, Serratosa JM, Sánchez MP (2012) Laforin and malin deletions in mice produce similar neurologic impairments. J Neuropathol Exp Neurol 71(5):413–421
17. Valles-Ortega J, Duran J, Garcia-Rocha M, Bosch C, Saez I, Pujadas L, Serafin A, Cañas X et al (2011) Neurodegeneration and functional impairments associated with glycogen synthase accumulation in a mouse model of Lafora disease. EMBO Mol Med 3:667–681
18. Aguado C, Sarkar S, Korolchuk VI, Criado O, Vernia S, Boya P, Sanz P, de Córdoba SR et al (2010) Laforin, the most common protein mutated in Lafora disease, regulates autophagy. Hum Mol Genet 19(14):2867–2876
19. Vernia S, Rubio T, Heredia M, Rodríguez de Córdoba S, Sanz P (2009) Increased endoplasmic reticulum stress and decreased proteasomal function in Lafora disease models lacking the phosphatase laforin. PLoS One 4(6):e5907
20. Vernia S, Solaz-Fuster MC, Gimeno-Alcañiz JV, Rubio T, García-Haro L, Foretz M, de Córdoba SR, Sanz P (2009) AMP-activated protein kinase phosphorylates R5/PTG, the glycogen targeting subunit of the R5/PTG-protein phosphatase 1 holoenzyme, and accelerates its down-regulation by the laforin-malin complex. J Biol Chem 284(13):8247–8255
21. Upadhyay M, Agarwal S, Bhadauriya P, Ganesh S (2017) Loss of laforin or malin results in increased Drp1 level and concomitant mitochondrial fragmentation in Lafora disease mouse models. Neurobiol Dis 100:39–51
22. Lahuerta M, Aguado C, Sánchez-Martín P, Sanz PKE (2018) Degradation of altered mitochondria by autophagy is impaired in Lafora disease. FEBS J 285(11):2071–2090
23. Romá-Mateo C, Aguado C, García-Giménez JL, Knecht E, Sanz P, Pallardó FV (2015) Oxidative stress, a new hallmark in the pathophysiology of Lafora progressive myoclonus epilepsy. Free Radic Biol Med 88:30–41
24. Berthier A, Payá M, García-Cabrero AM, Ballester MI, Heredia M, Serratosa JM, Sánchez MP, Sanz P (2016) Pharmacological interventions to ameliorate neuropathological symptoms in a mouse model of Lafora disease. Mol Neurobiol 53(2):1296–1309
25. Augé E, Pelegrí C, Manich G, Cabezón I, Guinovart JJ, Duran J, Vilaplana J (2018) Astrocytes and neurons produce distinct types of polyglucosan bodies in Lafora disease. Glia 66(10):2094–2107
26. Rubio-Villena C, Viana R, Bonet J, Garcia-Gimeno MA, Casado M, Heredia M, Sanz P (2018) Astrocytes: new players in progressive myoclonus epilepsy of Lafora type. Hum Mol Genet 27(7): 1290–1300
27. Lahuerta M, Gonzalez D, Aguado C, Fathinajafabadi A, García-Giménez JL, Moreno-Estellés M, Romá-Mateo C, Knecht E et al (2020) Reactive glia-derived neuroinflammation: a novel hallmark in Lafora progressive myoclonus epilepsy that progresses with age. Mol Neurobiol 57(3):1607–1621
28. Ransohoff RM (2016) How neuroinflammation contributes to neurodegeneration. Science (80-) 353(6301):777–783
29. Muñoz-Ballester C, Santana N, Perez-Jimenez E, Viana R, Artigas F, Sanz P (2019) In vivo glutamate clearance defects in a mouse model of Lafora disease. Exp Neurol 320:112959
30. Muñoz-Ballester C, Berthier A, Viana R, Sanz P (2016) Homeostasis of the astrocytic glutamate transporter GLT-1 is

altered in mouse models of Lafora disease. Biochim Biophys Acta 1862(6):1074–1083
31. Ortolano S, Vieitez I, Agis-Balboa RC, Spuch C (2014) Loss of GABAergic cortical neurons underlies the neuropathology of Lafora disease. Mol Brain 7:7
32. García-Cabrero AM, Sánchez-Elexpuru G, Serratosa JM, Sánchez MP (2014) Enhanced sensitivity of laforin- and malin-deficient mice to the convulsant agent pentylenetetrazole. Front Neurosci 8:291
33. Duran J, Gruart A, García-Rocha M, Delgado-García JM, Guinovart JJ (2014) Glycogen accumulation underlies neurodegeneration and autophagy impairment in lafora disease. Hum Mol Genet 23(12):3147–3156
34. Sánchez-Elexpuru G, Serratosa JM, Sanz P, Sánchez MP (2017) 4-Phenylbutyric acid and metformin decrease sensitivity to pentylenetetrazol-induced seizures in a malin knockout model of Lafora disease. Neuroreport 28(5):268–271
35. Bisulli F, Muccioli L, D'Orsi G, Canafoglia L, Freri E, Licchetta L et al (2019) Treatment with metformin in twelve patients with Lafora disease. Orphanet J Rare Dis 14:149
36. Brewer MK, Uittenbogaard A, Austin GL, Segvich DM, DePaoli-Roach A, Roach PJ et al (2019) Targeting pathogenic Lafora bodies in Lafora disease using an antibody-enzyme fusion. Cell Metab. 30(4):689–705.e6
37. Delpech JC, Madore C, Nadjar A, Joffre C, Wohleb ES, Layé S (2015) Microglia in neuronal plasticity: influence of stress. Neuropharmacology 96:19–28
38. Kota DJ, Prabhakara KS, van Brummen AJ, Bedi S, Xue H, DiCarlo B, Cox CS Jr, Olson SD (2016) Propranolol and medenchymal stromal cells combine to treat traumatic brain injury. Stem Cells Transl Med 5:33–44
39. Lin SY, Wang YY, Chang CY, Wu CC, Chen WY, Kuan YH, Liao SL, Chen CJ (2020) Effects of β-Adrenergic blockade on metabolic and inflammatory responses in a rat model of ischemic stroke. Cells 9(6):1373
40. Woiciechowsky C, Schöning B, Stoltenburg-Didinger G, Stockhammer F, Volk HD (2004) Brain-IL-1β triggers astrogliosis through induction of IL-6: inhibition by propranolol and IL-10. Med Sci Monit 10(9):325–330
41. Dobarro M, Gerenu G, Ramírez MJ (2013) Propranolol reduces cognitive deficits, amyloid and tau pathology in Alzheimer's transgenic mice. Int J Neuropsychopharmacol 16(10):2245–2257
42. Herges K, Millward JM, Hentschel N, Infante-Duarte C, Aktas O, Zipp F (2011) Neuroprotective effect of combination therapy of Glatiramer acetate and epigallocatechin-3-gallate in neuroinflammation. PLoS One 6(10):e25456
43. Cascella M, Bimonte S, Muzio MR, Schiavone V, Cuomo A (2017) The efficacy of Epigallocatechin-3-gallate (green tea) in the treatment of Alzheimer's disease: an overview of pre-clinical studies and translational perspectives in clinical practice. Infect Agent Cancer 12:36
44. Wang J, Li P, Qin T, Sun D, Zhao X, Zhang B (2020) Protective effect of epigallocatechin-3-gallate against neuroinflammation and anxiety-like behavior in a rat model of myocardial infarction. Brain Behav 10(6):1–9
45. Fischer W (2002) Anticonvulsant profile and mechanism of action of propanolol and its two enantiomers. Seizure 11(5):285–302
46. Lalonde R, Strazielle C (2011) Brain regions and genes affecting limb-clasping responses. Brain Res Rev 67(1–2):252–259
47. Steru L, Chermat R, Thierry B, Simon P (1985) The tail suspension test: a new method for screening antidepressants in mice. Psychopharmacology 85(3):367–370
48. Luong TN, Carlisle HJ, Southwell A, Patterson PH (2011) Assessment of motor balance and coordination in mice using the balance beam. J Vis Exp 49:2376
49. Matsuura K, Kabuto H, Makino H, Ogawa N (1997) Pole test is a useful method for evaluating the mouse movement disorder caused by striatal dopamine depletion. J Neurosci Methods 73(1):45–48
50. Korpi ER, Koikkalainen P, Vekovischeva OY, Mäkaela R, Kleinz R, Uusi-oukari M et al (1998) Cerebellar granule-cell-specific GABA A receptors attenuate benzodiazepine-induced ataxia : evidence from α 6-subunit-deficient mice. Eur J Neurosci 11:233–240
51. Sarnyai Z, Sibille EL, Pavlides C, Fenster RJ, McEwen BS, Tóth M (2000) Impaired hippocampal-dependent learning and functional abnormalities in the hippocampus in mice lacking serotonin1A receptors. Proc Natl Acad Sci U S A 97(26):14731–14736
52. Vogel-Ciernia A, Wood M (2014) Examining object localtion and object recognition memory in mice. Curr Protoc Neurosci 69: 8.31.1–8.31.17
53. Seese RR, Wang K, Yao YQ, Lynch G, Gall CM (2014) Spaced training rescues memory and ERK1/2 signaling in fragile X syndrome model mice. Proc Natl Acad Sci U S A 111(47):16907–16912
54. Can A, Dao DT, Terrillion CE, Piantadosi SC, Bhat S, Gould TD (2012) The tail suspension test. J Vis Exp 59:e3769
55. Calpe-López C, García-Pardo MP, Martínez-Caballero MA, Santos-Ortíz A, Aguilar MA (2020) Behavioral traits associated with resilience to the effects of repeated social defeat on cocaine-induced conditioned place preference in mice. Front Behav Neurosci 13(January):1–20
56. RStudio_Team (2020) RStudio: Integrated Development for R. RStudio. PBC, Boston
57. Cohen J (1988) Statistical power analysis for the behavioral sciences, 2nd edn. Erlbaum, Hillsdale
58. Kraemer HC, Morgan GA, Leech NL, Gliner JA, Vaske JJ, Harmon RJ (2003) Measures of clinical significance. J Am Acad Child Adolesc Psychiatry 42(12):1524–1529
59. López-González I, Viana R, Sanz P, Ferrer I (2017) Inflammation in Lafora disease: evolution with disease progression in Laforin and Malin knock-out mouse models. Mol Neurobiol 54(5):3119–3130
60. Felsky D, Roostaei T, Nho K, Risacher SL, Bradshaw EM, Petyuk V et al (2019) Neuropathological correlates and genetic architecture of microglial activation in elderly human brain. Nat Commun 10(1):1–12
61. Dutta S, Sengupta P (2016) Men and mice: Relating their ages. Life Sci 152:244–248
62. Taneja K, Ganesh S (2020) Dendritic spine abnormalities correlate with behavioral and cognitive deficits in mouse models of Lafora disease. J Comp Neurol. https://doi.org/10.1002/cne.25006
63. Navarro-Cruz AR, Ramírez Y, Ayala R, Ochoa-Velasco C, Brambila E, Avila-Sosa R, Pérez-Fernández S et al (2017) Effect of chronic administration of resveratrol on cognitive performance during aging process in rats. Oxidative Med Cell Longev 2017:1–8
64. Gao Q, Song H, Wang XT, Liang Y, Xi YJ, Gao Y et al (2017) Molecular hydrogen increases resilience to stress in mice. Sci Rep 7(1):1–12
65. Hodges-Savola C, Rogers SD, Ghilardi JR, Timm DR, Mantyh PW (1996) β-Adrenergic receptors regulate astrogliosis and cell proliferation in the central nervous system in vivo. Glia 17(1):52–62

Publisher's Note Springer Nature remains neutral with regard to jurisdictional claims in published maps and institutional affiliations.